

Hidden order and multipolar exchange striction in a correlated f -electron system

Leonid V. Pourovskii^{1,2} and Sergii Khmelevskyi³

¹*Centre de Physique Théorique, Ecole Polytechnique, CNRS,
Institut Polytechnique de Paris, 91128 Palaiseau Cedex, France*

²*Collège de France, 11 place Marcelin Berthelot, 75005 Paris, France*

³*Research Center for Computational Materials Science and Engineering,
Vienna University of Technology, Karlsplatz 13, 1040 Vienna, Austria*

Abstract

The nature of order in low-temperature phases of some materials is not directly seen by experiment. Such “hidden orders” (HO) may inspire decades of research to identify the mechanism underlying those exotic states of matter. In insulators, HO phases originate in degenerate many-electron states on localized f or d shells that may harbor high-rank multipole moments. Coupled by inter-site exchange, those moments form a vast space of competing order parameters. Here, we show how the ground state order and magnetic excitations of a prototypical HO system, neptunium dioxide NpO_2 , can be fully described by a low-energy Hamiltonian derived by a many-body *ab initio* force-theorem method. Superexchange interactions between the lowest crystal-field quadruplet of Np^{4+} ions induce a primary non-collinear order of time-odd rank-5 (triakontadipolar) moments with a secondary quadrupole order preserving the cubic symmetry of NpO_2 . Our study also reveals an unconventional multipolar exchange striction mechanism behind the anomalous volume contraction of the NpO_2 HO phase.

Significance statement

Second-order phase transitions in solids occur due to spontaneous symmetry breaking with an order parameter continuously emerging from the disordered high-temperature phase. In some materials, the phase transitions is clearly detected in thermodynamic functions (e.g., specific heat) but the microscopic order parameters remain “hidden” from researchers, in some cases for decades. Here we show how such hidden-order parameters can be unambiguously identified and the corresponding ordered phase fully described using a first-principles many-body linear-response theory. Considering the canonical “hidden-order” system neptunium dioxide, we also identify a novel mechanism of spontaneous multipolar exchange striction that induces an anomalous volume contraction of the hidden-order phase in NpO_2 .

Keywords: strongly correlated electrons; hidden order; *ab initio*; linear response; effective Hamiltonians

Spontaneous symmetry breaking, or a phase transition, in extended systems is associated with emergence of a macroscopic order parameter, which is the statistical average over some physical observable. In some systems the onset of order is clearly observed in the behavior of thermodynamic functions, however, the order parameter is not detectable by standard probes like neutron scattering or magnetic susceptibility measurements. In metals such phenomena are typically associated with strongly correlated heavy-fermion behavior, as in the case of enigmatic URu_2Si_2 .^{1–3} In correlated insulators HO phases typically originate in high-rank multipolar degrees of freedom on localized f and d -electron shells. It has been realized long time ago⁴ that in correlated magnetic insulators with strong spin-orbit coupling, apart from the ordinary Heisenberg interaction between localized spins, there may also exist inter-site interactions coupling higher order spin operators (magnetic multipoles). If those interactions are essentially large this might lead

to a new state of matter - a multipolar order without any associated magnetic order.^{5–7} Such purely multipolar orders have been observed in various f -electron^{2,8–11} and transition-metal correlated systems.^{12–14} Owing to numerous competing order parameters and small relevant energy scales, quantitative description of the HO represents a formidable challenge for theory. First-principles approaches to HO are typically restricted to simulations of few likely phases inferred experimentally and do not attempt to explore the full space of possible multipolar orders.^{1,15}

Difficulties of identifying the physical order parameter in a vast phase space of possible HOs are exemplified by the case of cubic NpO_2 .⁸ A sharp second order phase transition at $T_0 \simeq 26$ K was detected in NpO_2 more than half-century ago,¹⁶ with no evidence for underlying magnetic order and structural transformations,^{17–19} apart from a small anomalous contraction of the cubic unit cell volume observed²⁰ below T_0 . At the same time, NMR

measurements²¹ detect two inequivalent oxygen sites in the unit cell below T_0 , due to lowering of the cubic symmetry from high-temperature $Fm\bar{3}m$ to $Pn\bar{3}m$ by a longitudinal order of Np quadrupoles. However, a primary quadrupolar order parameter initially suggested²² is excluded since muon spin-rotation measurements detect a non-zero magnetic density.²³ Moreover, the crystal-field (CF) ground state quadruplet Γ_8 is split in the HO phase into two singlets and a doublet suggesting a time-odd primary order parameter.^{19,24,25} There is a multitude of possible high-rank odd order parameters realizable within the $J=9/2$ ground state multiplet of Np^{4+} ($J=3,5,7$, i.e. octupolar, triakontadipolar, etc.). A lot of efforts has been directed over the last two decades^{21,23,24,26-29} to identify a possible primary order able to reconcile various experimental facts. In particular, assumption of a triakontadipolar AF $3\mathbf{k}$ order of the Γ_5 symmetry was shown^{24,25,30} to lead to the best agreement with X-ray scattering and inelastic neutron scattering (INS) spectra. The same hypothesis is also strongly supported by estimates of the relative strength of odd Γ_5 multipole moments on the Np f^3 shell in the presence of CF splitting.^{24,31}

Though there are substantial experimental evidences to support the $3\mathbf{k}$ rank-5 order in NpO_2 , the mechanism of its formation is still not well understood. The simplest possible form of the superexchange (SE) Hamiltonian, consisting of diagonal nearest-neighbor interactions between three Γ_5 triakontadipoles and between three dipole moments, has been employed in analysis of low-temperature susceptibility and INS data.^{24,25} The full structure of this Hamiltonian cannot be extracted from experiment due to a large number of possible SE interactions (SEI). The measured CF splitting of 55 meV between the Γ_8 ground-state and first excited CF level^{8,19,32} is much larger than T_0 , suggesting SEI between Γ_8 states on neighboring Np ions as the origin of its exotic ordered phase. Such low-energy SE Hamiltonian has not been so far derived theoretically. Previous theoretical density-functional-theory+U (DFT+U) studies have confirmed the stability of a triakontadipolar order in NpO_2 ,^{15,33} however, they imposed an initial symmetry breaking consistent with the $3\mathbf{k}$ rank-5 order inferred experimentally.

In this work we apply a novel framework to the problem of "hidden" multipolar orders in correlated insulators as exemplified by NpO_2 . It consists in evaluating the full low-energy SE Hamiltonian from an *ab initio* description of the symmetric paramagnetic phase. We start with charge-self consistent DFT+dynamical mean-field theory³⁴⁻³⁶ calculations for paramagnetic NpO_2 treating Np $5f$ within the quasi-atomic Hubbard-I (HI) approximation³⁷ (this method is abbreviated below as DFT+HI) to obtain its electronic structure and the composition of a CF-split Np $5f^3$ shell. A force theorem approach,³⁸ abbreviated FT-HI, is subsequently employed to derive SEIs between the calculated CF Γ_8 ground-state quadruplets. Our study represents first, to our awareness, *ab initio* electronic structure calculation of

a complete SE Hamiltonian for high-rank magnetic multipoles in an f -electron crystalline material. By solving this Hamiltonian, we find a $3\mathbf{k}$ rank-5 primary magnetic multipolar order (MMO) accompanied by a secondary longitudinal quadrupole order. The calculated time-odd splitting of Γ_8 and magnetic excitation spectra are in a good agreement with experiment. The lattice contraction effect²⁰ is shown to be not related to quadrupole ordering as suggested before,³⁹ but rather to stem from the volume dependence of leading time-odd SEIs. This multipolar "exchange-spring" effect is quite unique and has not been, to our awareness, discussed previously in the literature. Overall, we show that within our first-principles scheme, which treats all competing order parameters on the equal footing, high-rank multipolar orders in correlated insulators can be captured both qualitatively and quantitatively.

RESULTS

Crystal-field splitting and super-exchange Hamiltonian

We start with evaluating the Np CF splitting in paramagnetic NpO_2 ; as discussed above, this splitting determines the space of low-energy states forming the MMO. The CF splitting of the Np $5f^3$ ground state multiplet $J=9/2$ calculated by DFT+HI is shown in Fig.1a. The ground state Γ_8 quartet is separated from another, excited, Γ_8 quartet by 68 meV, in agreement with the experimental range for this splitting, 30-80 meV, inferred from INS measurements.^{19,32,40} The broad experimental range for the excited Γ_8 energy is due to the presence of a dispersive phonon branch in the same range (this overlap has been a major source of difficulties for the phenomenological analysis of the NpO_2 in the framework of crystalline effective field model⁸). Third excited level, Γ_6 doublet, is located at much higher energy above 300 meV.

Our calculated CF corresponds to $x=-0.54$ parameterizing the relative magnitude of the 4 and 6-order contributions to the cubic CF.⁴¹ Our values are in good agreement with $x=-0.48$ inferred from INS measurements¹⁹ and analysis of CF excitation energies along the actinide dioxide series.³¹ The CF level energies calculated within DFT+HI are also in good agreement with previous DFT+DMFT calculations by Kolorenč *et al.*⁴² employing an exact diagonalization approach to Np $5f$. The calculated wavefunctions of the CF ground-state Γ_8 quartet (see Supplementary Table I) feature a small admixture of the excited $J=11/2$ and $13/2$ multiplets.

The space of CF GS Γ_8 quadruplet is conveniently represented by the effective angular momentum quantum number $J_{eff}=3/2$, with the Γ_8 wave functions (WFs) labeled by the corresponding projection $M=-3/2\dots+3/2$ and the phases of WFs chosen to satisfy the time-reversal symmetry (see Supplementary Table I). The on-site degrees of freedom within the GS quadruplet are (pseudo)

dipole, quadrupole, and octupole moments defined for $J_{eff}=3/2$ in the standard way.⁸ Hence, the most general form for a SE coupling between Γ_8 quadruplets on two Np sites reads

$$\sum_{KK'Q'Q''} V_{KK'}^{QQ'}(\mathbf{R}) O_K^Q(\mathbf{R}_0) O_{K'}^{Q'}(\mathbf{R}_0 + \mathbf{R}), \quad (1)$$

where $O_K^Q(\mathbf{R}_0)$ and $O_K^Q(\mathbf{R}_0 + \mathbf{R})$ are the real spherical tensor operators⁸ for $J=3/2$ of rank $K=1, 2$, or 3 , $-K \leq Q \leq K$, acting on the site \mathbf{R}_0 and $\mathbf{R}_0 + \mathbf{R}$, respectively, $V_{KK'}^{QQ'}(\mathbf{R})$ is the SEI that couples them; due to the translational invariance, $V_{KK'}^{QQ'}$ depends only on the intersite lattice vector \mathbf{R} .

We employed the FT-HI approach³⁸ to evaluate all interactions $V_{KK'}^{QQ'}(\mathbf{R})$ from the converged DFT+HubI NpO₂ electronic structure for several first Np coordination shells. Only nearest-neighbor (NN) SEIs are significant, with longer distance ones being more than an order of magnitude smaller. All SEIs $V_{KK'}^{QQ'}(\mathbf{R})$ for a given bond \mathbf{R} form a matrix, designated below as the SEI matrix, with the rows and columns labeled by the moments KQ and $K'Q'$ on the sites \mathbf{R}_0 and $\mathbf{R}_0 + \mathbf{R}$, respectively. The NN SEI matrix $\hat{V}(\mathbf{R})$ is graphically represented in Fig. 1b (see also Supplementary Table II) using a local coordinate system with the quantization axis $z \parallel \mathbf{R}$. This 15×15 matrix is of a block-diagonal form, since the interactions between time-even and time-odd moments are zero by symmetry. It can thus be separated into the dipole-dipole (DD), quadrupole-quadrupole (QQ), octupole-octupole (OO), and dipole-octupole (DO) blocks. In spite of this simplification, the SEI matrix \hat{V} can in principle contain 70 distinct elements. The number of distinct non-zero matrix elements in \hat{V} , while reduced by the cubic symmetry to 38, remains rather large.

Our calculations predict the largest values for the diagonal DD $x-x$ (AF, 1.6 meV) SEI. However, the off-diagonal OO xyz to $y(x^2 - 3y^2)$ (ferro, -1.5 meV) and DO z to z^3 (AF, 0.95 meV) couplings are of about the same magnitude as the DD $x-x$ one. Overall, the calculated \hat{V} matrix shown in Fig. 1b features many non-negligible DD, OO, and DO interactions of a comparable magnitude. The QQ interactions are weaker reflecting the secondary nature of the quadrupole order. Our calculations thus predict a complex and frustrated SE in NpO₂, which may give rise to multiple competing time-odd orders. Therefore, as has been previously noted,^{8,25} extracting a full SE Hamiltonian of NpO₂ from experimental (e. g., INS) data is virtually impossible due to a large number of parameters entering into the fit of an excitation spectra. The same difficulty is encountered by *ab initio* approaches based on total energy calculations for symmetry broken phases,^{15,33,43} which require a large number of very precise calculations to extract multiple non-negligible matrix elements of \hat{V} , with the magnitude of 0.5 meV and above. Within the present framework all interactions are extracted from a single *ab initio* calculation for paramagnetic NpO₂.

Ordered state of NpO₂

The calculated SE Hamiltonian for NpO₂ reads

$$H_{SE} = \frac{1}{N} \sum_{\mathbf{R} \in \text{NN}} \hat{O}(\mathbf{R}_0) \hat{V}(\mathbf{R}) \hat{O}(\mathbf{R}_0 + \mathbf{R}), \quad (2)$$

where \mathbf{R} runs over all NN bonds in the Np fcc sublattice, N is the number of Np sites, and we also introduced the obvious vector notation $\hat{O} \equiv [\hat{O}_1^{-1}, \dots, \hat{O}_3^3]$ for multipole tensors. The SEI matrix $\hat{V}(\mathbf{R})$, eq. 1, is that in the local frame $\mathbf{R} \parallel z$ (Fig. 1b) rotated to align \mathbf{R} along the corresponding Np NN bond. We solved (2) numerically within the mean-field (MF) approximation, obtaining a second-order transition at $T_0=38$ K, in good agreement with its experimental value of 26 K taking into account the usual mean-field overestimation of ordering temperatures. The numerical results were verified by a linearized (MF) theory, derived by first-order expansion of MF equations in the order parameters $\langle \hat{O} \rangle$, see Method section.

The resulting GS order of NpO₂ in the J_{eff} space consists of a primary (pseudo) dipole-octupole order combined with secondary (pseudo) quadrupole one (see Supplementary Table III for the values of all J_{eff} order parameters and Supplementary Figure 1). The pseudo-dipole order is a complex $3\mathbf{k}$ planar AF structure, with four inequivalent simple-cubic sublattices forming two pairs with different moment magnitude; the moments of those two pairs are aligned along the $\langle 1, 1, 0 \rangle$ and $\langle 3, 1, 0 \rangle$ directions in the fcc lattice, respectively. The origin of this inclined AF structure of pseudo-dipoles is in the dipole-octupole SEI; similarly to physical AF magnetic orders found in some materials with large SO that are likely induced by higher-order magnetic multipolar interactions. The pseudo-octupoles order is also oriented in non-symmetrical directions. The secondary pseudo-quadrupole order is of a $3\mathbf{k}$ type, which we analyze in details below.

We subsequently mapped the moments calculated in the $J_{eff} = 3/2$ space into the observable multipolar moments that are defined in the physical $J = 9/2$ space of Np $5f^3$ GS multiplet (see Methods). The calculated physical multipole order of NpO₂ is displayed in Fig. 2. Notice, that observable moments up to $K=7$ can exist on an f -electron shell;⁸ we show the largest primary (odd) and secondary (even) order parameters as well as the physically important quadrupole order. All non-zero multipole moments are listed in Supplementary Table IV. The physical dipole magnetic moments are found to completely vanish, since their contribution into the $\langle O_x \rangle$ and $\langle O_y \rangle$ pseudo-dipole $J_{eff} = 3/2$ moments is exactly canceled by that due to the $\langle T_x \rangle$ and $\langle T_y \rangle$ pseudo-octupoles. The primary order parameter is of rank-5 (triakontadipole); the physical octupole moments is an order of magnitude smaller and the magnitude of rank-7 moments is about 1/3 of that for triakontadipoles, in agreement with previous estimates for the relative contribution of those multipoles into the MMO order in NpO₂.²⁴ The

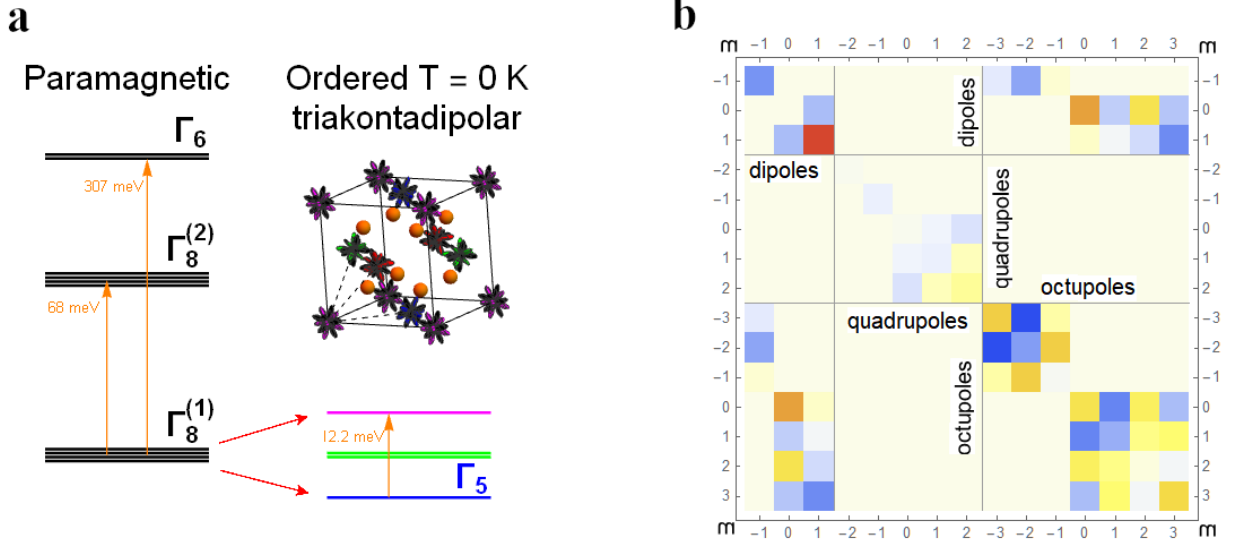


FIG. 1: **Np $5f$ on-site splitting and Np-Np inter-site interactions in NpO_2 .** (a) Calculated crystal-field (CF) splitting of Np $5f^3$ $J=9/2$ multiplet in paramagnetic state (left) and exchange splitting of the ground state quartet in the predicted ordered phase at zero temperature (right). Note the energy rescaling for the Γ_6 level on the CF splitting plot. Inset: the crystal structure of the NpO_2 . Positions of the Np-atoms is surrounded by the polar plot of the calculated primary order parameter (triakontadipoles) in the ground state. Different colors indicate four non-equivalent Np positions in the ordered state. The orange spheres are oxygen atoms. (b) SEI matrix between nearest-neighbor Np in NpO_2 . These SEI couple multipolar operators \hat{O}_{lm} in the $J_{eff}=3/2$ space of the Γ_8 CF ground state. Their values in the local coordinate system (with z-axis directed along the given bond direction and y-axis along the edge of the fcc lattice) are presented as a temperature map with the warm and cool colors representing, respectively, antiferromagnetic and ferromagnetic coupling of the corresponding multipoles.

magnetic triakontadipoles on different sublattices are oriented in four different directions (forming mutual angles corresponding to the angles between the cube's main diagonals) thus structure similarly to the $3\mathbf{k}$ -AFM dipole order in UO_2 , see Fig. 2a. The secondary order is dominated by hexadecapole (rank-4), Fig. 2b; the ordered quadrupole moments (Fig. 2c) are roughly twice smaller. The quadrupole order is directly related to the pseudo-quadrupole one, since the Γ_5 (or t_{2g}) pseudo-quadrupoles directly map into the physical ones, apart from swapping $xy \leftrightarrow yz$ and $x^2 - y^2 \leftrightarrow xz$. The resulting physical quadrupole order can be represented, in the space of Γ_5 quadrupoles $[O_{yz}, O_{xz}, O_{xy}]$, by four directions $[\bar{1}11]$, $[1\bar{1}\bar{1}]$, $[11\bar{1}]$, and $[\bar{1}\bar{1}1]$ for four inequivalent Np sublattices $[0,0,0]$, $[1/2,1/2,0]$, $[1/2,0,1/2]$, and $[0,1/2,1/2]$, respectively. These quadrupoles can be depicted as $\langle O_{z^2} \rangle$ moments with the principal axes z along the corresponding direction at each given site (Fig. 2c). One sees that the ordered quadrupoles on the four Np sites forming the tetrahedron around each oxygen can either have their principal axes directed along the Np-O bonds towards the central O, or form the same angle of 70.5° with respect to those bonds. In both cases the tetrahedron symmetry is preserved. The first case is realized for two O along one of the principal cubic diagonals, while the second one is found for 6 others, resulting in the lowering of NpO_2 symmetry to $Pn\bar{3}m$ from $Fm\bar{3}m$ without any distortion

of the cubic structure. This longitudinal $3\mathbf{k}$ quadrupole order, previously proposed on the basis of resonant x-ray scattering,³⁰ and subsequently confirmed by the splitting of ^{17}O -NMR spectra in ordered NpO_2 ,²¹ is thus predicted by our *ab initio* SE Hamiltonian (2).

Exchange splitting and magnetic excitations

Having obtained the MMO of NpO_2 we subsequently calculated its excitation spectra, which has been previously measured, in particular, by INS.^{19,25}

The MMO lifts the degeneracy of CF GS Γ_8 quartet, the resulting exchange splitting calculated from the *ab initio* SE Hamiltonian (2) is depicted on the right panel of Fig. 1a. The ground state is a Γ_5 singlet with the first excited doublet found at 6.1 meV above the GS Γ_5 singlet and the second excited level, singlet, located at 12.2 meV. The calculated position of first excited doublet is in excellent agreement with the location of a prominent peak in INS spectra at about 6.4 meV¹⁹ in the ordered phase; another broad excitation was observed in the range of 11-18 meV,²⁵ see below. Previously, an exchange splitting of the Γ_8 was obtained assuming a diagonal uniform SEI between Γ_5 triakontadipoles tuned to reproduce the experimental position of the excited doublet,²⁴ thus obtained energy for the excited singlet is in agreement with

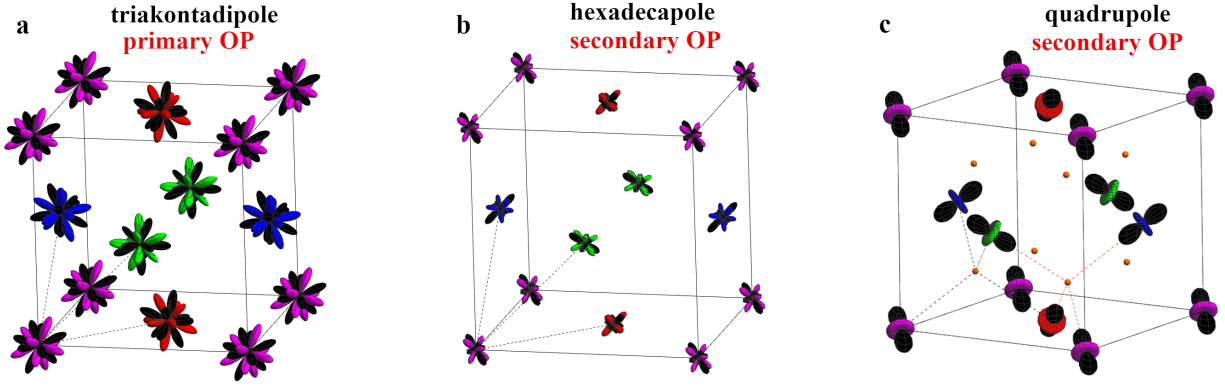


FIG. 2: **Calculated multipolar order in NpO_2 .** This order of the physical multipoles in NpO_2 derived by mapping of the $J_{\text{eff}} = 3/2$ space to the full $J = 9/2$ space. The physical magnetic dipoles (magnetic moments) are exactly canceled on all Np sites, resulting in a purely multipolar order. (a) The primary physical order parameter, $K = 5$ triakontadipole (b) The largest secondary “slave” order parameter, $K = 4$ hexadecapole. The displayed isovalue for the primary and secondary order parameters is normalized with respect to the maximum possible value of a given moment in the Γ_8 crystal-field ground-state quartet. Hence the relative size of plotted moments indicates their relative magnitude. Black dashed lines are the primitive lattice translations of the original Np cubic face-centered sublattice, which in the ordered phase connect inequivalent Np sublattices. (c) Longitudinal $3\mathbf{k}$ order of “slave” quadrupole moments, which are scaled on the plot by a factor of 4. Np-O bonds for two inequivalent O sites (small orange balls) in ordered NpO_2 are indicated by dashed lines. One sees that in the Np tetrahedron around each O all ordered Np quadrupoles are directed either along the Np-O bonds, or form the same angle with those bonds. This longitudinal $3\mathbf{k}$ quadrupolar order preserves the cubic positions of oxygen sites in the ordered phase of NpO_2 , in contrast to the transverse $3\mathbf{k}$ quadrupole order in UO_2 .

our *ab initio* result.

We also calculated the theoretical INS cross-section, $\frac{d^2\sigma(\mathbf{q}, E)}{dE d\Omega} = S(\mathbf{q}, E) \propto \sum_{\alpha, \beta} \left(\delta_{\alpha\beta} - \frac{q_\alpha q_\beta}{q^2} \right) \text{Im} \chi_{\alpha\beta}(\mathbf{q}, E)$, where $E(\mathbf{q})$ the energy (momentum) transfer, respectively, $\alpha(\beta) = x, y, z$, and $\chi_{\alpha\beta}(\mathbf{q}, E)$ is the dynamical magnetic susceptibility. The latter was evaluated within the random-phase approximation (RPA) from the full calculated *ab initio* SE Hamiltonian (2), see Methods. The resulting INS spectra $S(\mathbf{q}, E)$ for \mathbf{q} along high-symmetry directions of the fcc lattice is displayed in Fig. 3a. Along the $\Gamma - X$ path it is similar to that previously calculated from the simplified empirical SE Hamiltonian of Ref. 24. The $S(\mathbf{q}, E)$ structure is richer along other directions showing multiple branches in the E range from 4 to 8 meV. The experimental INS spectra $S(\mathbf{q}, E)$ has not been measured so far due to lack of large single-crystal samples,⁸ hence, our result represents a prediction for future experiments. The calculated spherically averaged INS cross-section $\int S(\mathbf{q}, E) d\hat{q}$ is compared in Fig. 3b with that measured²⁵ on powder samples at the same $|q| = 2.5 \text{ \AA}^{-1}$. The theoretical INS spectra exhibits prominent peaks at around 6 meV and at about 12.5 meV, corresponding to the transition from the Γ_5 GS to the excited doublet and singlet, respectively.

The theoretical low-energy feature agrees very well with the measured INS spectra, once experimental broadening is taken into account, see Fig. 3b. The high-energy feature, though, is clearly split in experiment into two broad peaks centered at about 12 and 16 meV, re-

spectively. In order to understand whether the relative weights of the low and high energy features is captured in the theory we employed the same analysis as Magnani *et al.*²⁵ Namely, we evaluated, as a function of the momentum transfer, the ratio of high-energy feature spectral weight to that of the low-energy one. The calculated ratio is in an excellent agreement with experiment up to $|q| = 2.5 \text{ \AA}^{-1}$. As noticed in Ref. 25, a phonon contribution to INS appears below 18 meV for large $|q|$ thus rendering the separation of magnetic and phonon scattering less reliable for $|q| > 2 \text{ \AA}^{-1}$. The splitting of high-energy peak was clearly observed at all measured $|q|$; it was not reproduced by the simplified semi-empirical SEI employed by Magnani *et al.* They speculated that this splitting might stem from complex realistic Np-Np SEIs, which they could not determine from experiment. In the present work we determined the full SE Hamiltonian for the GS CF Γ_8 quadruplet. Hence, the fact that the splitting of INS high-energy feature is still not reproduced points out to its origin likely being a SE coupling between the ground-state and first excited Γ_8 quadruplets (a significant contribution of the very high-energy Γ_6 CF doublet is unlikely). This inter-quadruplet coupling can be in principle derived using the present framework; we have not attempted to do this in the present work.

Alternatively, lattice mediated interactions might be also considered as the origin of the high-peak splitting. Those interactions couple time-even moments, i. e., the quadrupoles within the J_{eff} space. However, the

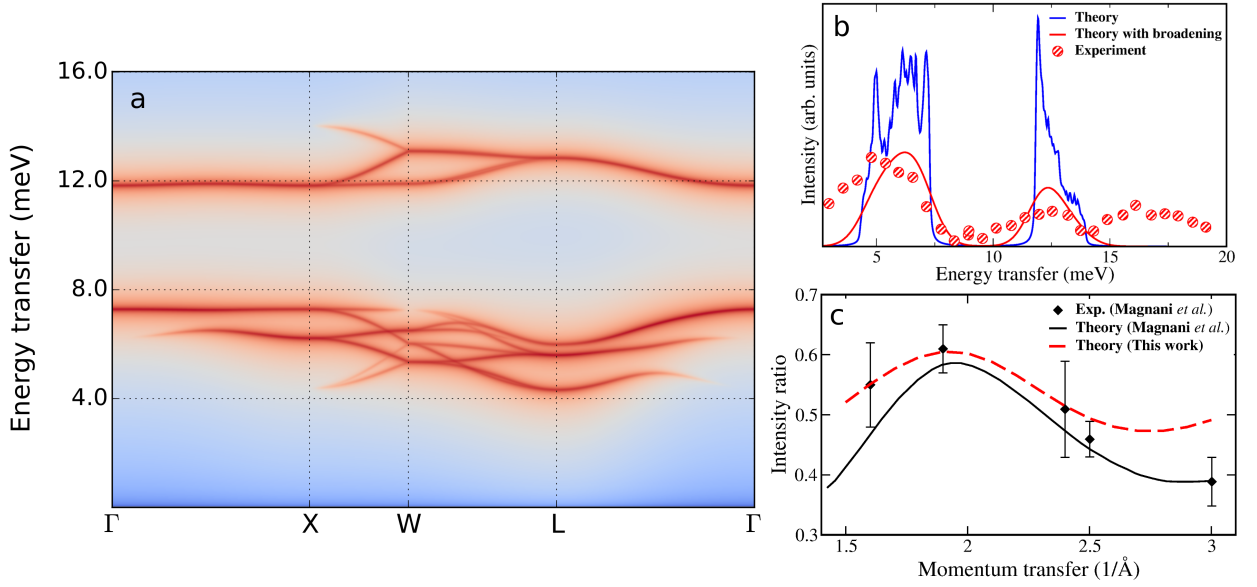


FIG. 3: **Inelastic neutron-scattering (INS) spectra in ordered NpO₂.** (a) INS cross-section $S(\mathbf{q}, E)$ with the momentum transfer \mathbf{q} along a high-symmetry path in the fcc Brillouin zone. The special points are $\Gamma = [0,0,0]$, $X = [1,0,0]$, $W = [1, \frac{1}{2}, 0]$, $L = [\frac{1}{2}, \frac{1}{2}, \frac{1}{2}]$, in units of $2\pi/a$. (b) Powder (spherically averaged) INS cross-section vs. energy transfer E for $|q| = 2.5 \text{ \AA}^{-1}$. The theoretical spectra was broadened with the Gaussian resolution function of 1.5 meV. The experimental points are from Magnani *et al.*²⁵ (c) Ratio of the spectral weights of the low-energy (around 6 meV) and high-energy (10-20 meV) features vs. momentum transfer in the powder INS spectra (panel b). The experimental points are from Magnani *et al.*²⁵ Theoretical points from the same work are calculated with a semi-empirical SE Hamiltonian, see text.

QQ coupling is rather expected to impact the shape of low-energy peak in Fig. 3b, since the corresponding lowest on-site excitation in the ordered phase (inset in Fig. 1a) is due to reverting of the on-site quadrupole moment.²⁴ Indeed, we recalculated the theoretical INS spectra (Fig. 3b) with the magnitude of QQ block in the SEI (Fig. 1b) scaled by a factor from 0 to 5. These variations of the QQ coupling strength do modify the shape of low-energy peak but have no impact on the high-energy one. Since the lattice-mediated coupling is expected to modify exclusively the QQ block, it is thus quite unlikely to be the origin of the splitting.

Multipolar exchange striction

The onset of the “hidden order” phase NpO₂ is marked by an anomalous volume contraction vs. decreasing temperature (anti-Invar anomaly). The estimated total volume contraction in the ordered state as compared to the paramagnetic phase is 0.018% at zero temperature.²⁰ This effect cannot be attributed to the conventional volume magnetostriction, since ordered magnetic moments are absent in NpO₂. Hence, this anomaly was speculated³⁹ to be induced by a (secondary) quadrupole order coupling to the lattice. As we show below, this is not the case, and the volume contraction in NpO₂ rather stems from the volume-dependent SEI coupling

high-rank magnetic multipoles.

In order to make a quantitative estimation for this anomaly we evaluated the volume dependence of NpO₂ ordering and elastic energies. To that end we adopted the elastic constants calculated for NpO₂ in the framework of DFT+U+SOC approach:⁴⁴ $C_{11} = 404 \text{ GPa}$, $C_{12} = 143 \text{ GPa}$. The corresponding parabolic volume dependence of elastic energy $E_{elast} = 1/3 (C_{11}/2 + C_{12}) \epsilon^2 \equiv K_{el} \epsilon^2$ where $\epsilon = (V - V_0)/V_0$ is the volume contraction, V_0 is the NpO₂ equilibrium volume,⁴⁴ is depicted in Fig. 4. The dependence of MMO energy vs. volume was obtained by calculating the SEIs at a few different volumes and then evaluating the mean-field order and ordering energy vs. volume expansion or contraction. The SE ordering energy remains linear vs. ϵ in a rather large range ($\epsilon = \pm 1\%$); its dependence upon ϵ for the relevant range of small ϵ is thus easily obtained.

As is seen in Fig. 4, the SE contribution shifts the equilibrium volume in the ordered state towards smaller volumes. The negative slope for the ordering energy vs. volume is expected as the SEIs become larger with decreasing Np-Np distance. Thus the multipolar SEIs act as springs (see scheme in Fig. 4 inset) pulling Np atoms closer as the order parameters increase below T_0 . Our approach is thus able to qualitatively capture this very small in magnitude subtle effect: the calculated spontaneous multipolar exchange striction is 0.023 % (Fig. 4) at zero T as compared to experimental estimate

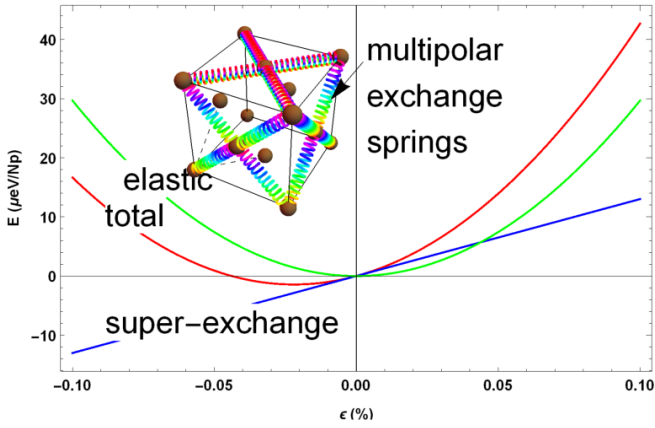


FIG. 4: **Multipolar exchange striction in NpO_2 .** The curves represent the DFT+U elastic energy (green), ordering energy of the multipolar ground state vs. volume (blue), the latter is calculated from the volume-dependent *ab initio* super-exchange interactions. The multipolar order is seen to induce the contraction of the equilibrium volume (total energy, red curve) due to the two-site multipolar striction effect, analogously to the two-site volume magnetostriction in conventional magnetically ordered materials. The “springs” in inset schematically illustrate the action of the intersite super-exchange energy upon the onset of NpO_2 multipolar order.

of 0.018%.^{20,45}

We also performed the same calculations suppressing the quadrupole-quadrupole SE obtaining only a minor change, by about 5%, in the slope of MMO energy vs. volume. Hence, the secondary quadrupole order plays virtually no role in the anomalous volume contraction. The physical origin of this effect is the volume dependence of leading, time-odd SEIs.

To analyze the temperature dependence of the anomalous contraction, one may recast the linear-in-volume MMO energy (Fig. 4) into a general form of $K_{SEI}^{pr} \epsilon \xi_{pr}^2(T) + K_{SEI}^{sec} \epsilon \xi_{sec}^2(T)$, where $\xi_{pr}(T)$ and $\xi_{sec}(T)$ are primary and secondary order parameters, respectively, K_{SEI}^{pr} and K_{SEI}^{sec} are the slopes of volume dependence for the corresponding contributions to MMO energy. The temperature dependence of the anomalous volume contraction is thus given by that of squares of the order parameters, $\xi_{pr}^2(T)$ and $\xi_{sec}^2(T)$. As shown in Supplementary Fig. 2, secondary quadrupole $\xi_{sec}^2(T)$ exhibits a smooth evolution across T_0 and rather slowly increase vs. decreasing T , while primary time-odd $\xi_{pr}^2(T)$ features a discontinuity in the slope at T_0 , as expected, with a rapid growth for $T < T_0$, reaching about 60% of total magnitude at $3/4T_0$. This behavior of $\xi_{pr}^2(T)$ is in a perfect agreement with the shape of temperature dependence of the volume anomaly,²⁰ thus confirming that it is induced directly by the time-odd primary order.

DISCUSSION

In conclusion, we have applied an advanced *ab initio* framework to the “hidden-order” phase of Neptunium dioxide NpO_2 . Our framework is based on the density-functional+dynamical mean-field theory (DFT+DMFT) in conjunction with a quasi-atomic approximation to local correlations on Np 5*f*. Its crucial part is a force-theorem method³⁸ that we employ to calculate super-exchange interactions between all multipole moments of the Np f^3 lowest crystal-field (CF) manifold. From the resulting super-exchange Hamiltonian we derive all order parameters of the “hidden-order” phase, its ordering temperature, magnetic excitations and volume effect. In fact, numerous properties of the NpO_2 “hidden-order” phenomenon that have been painstakingly determined in experiments over several decades – absence of conventional magnetic order, the CF level scheme, the primary triadicapole order and secondary longitudinal $3\mathbf{k}$ quadrupole order, the singlet-doublet-singlet exchange splitting of the CF ground state, the two-peak structure of the magnetic-excitation spectra – all of them are reproduced by our calculations that contain essentially no adjustable parameters. Therefore, the present scheme is shown to provide full, parameter-free and quantitatively correct description of super-exchange in complex realistic correlated insulators. On the basis of our theory we may also identify the features that are not stemming from the inter-site coupling between the ground-state CF levels. For example, the splitting of the high-energy peak in NpO_2 inelastic neutron scattering spectra likely stems from a super-exchange interaction with excited CF levels. We also uncover an unconventional mechanism for the anomalous volume contraction observed in ordered NpO_2 ; which is induced not by the secondary quadrupole order coupling to the lattice as previously assumed, but rather by the volume dependence of leading time-odd super-exchange interactions.

This first-principles methodology – a dynamical mean-field treatment of symmetric paramagnetic phase combined with the force-theorem extraction of the full complex inter-site exchange responsible for the spontaneous symmetry breaking – can be applied to a wide range of rare-earth, actinide and heavy transition-metals correlated systems,^{2,8,9,46} in which the interplay of a large spin-orbit coupling with crystalline environment gives rise to a large degeneracy of the crystal-field ground state and high-rank multipole moments. “Hidden” orders, stemming from coupling between those moments, can be predicted and their interplay with various parameters – external or chemical pressure, applied field, lattice distortions – identified, thus opening up an avenue for theoretical search of new exotic phases of matter.

METHODS

DFT+HI first-principles calculations. Our charge self-consistent DFT+DMFT calculations using the Hubbard-I (HI) approximation for Np $5f$, abbreviated as DFT+HI, were carried out for the CaF_2 -type cubic structure of NpO_2 with the experimental lattice parameter $a = 5.434 \text{ \AA}$. We employed the Wien-2k full-potential code⁴⁷ in conjunction with "TRIQS" library implementations for the DMFT cycle^{36,48} and HI. The spin-orbit coupling was included in Wien2k within the standard second-variation treatment. The Brillouin zone (BZ) integration was carried out using 1000 \mathbf{k} -points in the full BZ and the local density approximation (LDA) was employed as DFT exchange-correlation potential.

The Wannier orbitals representing Np $5f$ states were constructed by the projective technique of Refs. 49 and 50 using the Kohn-Sham bands enclosed by the energy window $[-2.04 : 2.18] \text{ eV}$ around the Kohn-Sham Fermi energy; this window thus encloses all Np $5f$ -like bands. The use of a narrow window enclosing only the target ($5f$ -like) band for the construction of local orbitals results in a so-called "extended" Wannier basis. By employing such a basis within DFT+HI one may effectively include the contribution of hybridization to the crystal-field splitting on localized shells, as discussed in ref.⁵¹ The same choice for the local $5f$ basis was employed in our previous DFT+HI study⁵² of UO_2 , resulting in a good quantitative agreement of the calculated CF splitting with experiment.

The on-site Coulomb interaction between Np $5f$ was specified by the Slater parameter $F_0 = 4.5 \text{ eV}$ and the Hund's rule coupling $J_H = 0.6 \text{ eV}$; the same values were previously employed for UO_2 .⁵² The double-counting correction was computed using the fully localized limit (FLL)⁵³ with the atomic occupancy of Np f^3 shell.⁵⁴ The DFT+DMFT charge self-consistency was implemented as described in Ref. 55. In our self-consistent DFT+HI calculations, we employed the spherical averaging of the Np $5f$ charge density, following the approach of Delange *et al.*,⁵⁶ in order to suppress the contribution of LDA self-interaction error to the crystal field. The DFT+HI calculations were converged to $5 \mu\text{Ry}$ in the total energy.

Crystal-field and superexchange interactions. The self-consistent DFT+HI calculations predict a crystal-field (CF) split $^4\text{I}_{9/2}$ atomic multiplet to have the lowest energy, in agreement with Hund's rules for an f^3 shell; the calculated spin-orbit coupling $\lambda = 0.27 \text{ eV}$. The predicted in these calculations CF splitting of the $^4\text{I}_{9/2}$ multiplet is shown in Fig. 1a and the corresponding CF wavefunctions are listed in Supplementary Table I. The cubic CF parameters $-A_4^0\langle r^4 \rangle = -152 \text{ meV}$, $A_4^4\langle r^4 \rangle = 5A_4^0\langle r^4 \rangle$, $A_6^0\langle r^6 \rangle = 32.6 \text{ meV}$, and $A_6^4\langle r^6 \rangle = 21A_6^0\langle r^6 \rangle$ – were extracted by fitting the converged DFT+HI one-electron $5f$ level positions.⁵⁶

The states of the CF ground-state quadruplet Γ_8 were

labeled by projection M of the pseudo-angular quantum number $J_{eff} = 3/2$ as specified in Supplementary Table I. We subsequently employed the FT-HI method³⁸ to evaluate all SEIs between the $J_{eff} = 3/2$ quadruplet for several first Np-Np coordination shells. Previously the FT-HI method has been applied to systems with conventional magnetic primary order.^{52,57} Within this method matrix elements of inter-site coupling $V^{\mathbf{R}}$ for the Np-Np bond \mathbf{R} read:

$$\langle M_1 M_3 | V^{\mathbf{R}} | M_2 M_4 \rangle = \text{Tr} \left[G_{\mathbf{R}} \frac{\delta \Sigma_{\mathbf{R}_0 + \mathbf{R}}^{at}}{\delta \rho_{M_3 M_4}^{\mathbf{R}_0 + \mathbf{R}}} G_{-\mathbf{R}} \frac{\delta \Sigma_{\mathbf{R}_0}^{at}}{\delta \rho_{M_1 M_2}^{\mathbf{R}_0}} \right], \quad (3)$$

where $\rho_{\mathbf{R}_0}^{M_i M_j}$ is the corresponding element of the $J_{eff} = 3/2$ density matrix on site \mathbf{R}_0 , $\frac{\delta \Sigma_{\mathbf{R}_0}^{at}}{\delta \rho_{M_i M_j}^{\mathbf{R}_0}}$ is the derivative of atomic (Hubbard-I) self-energy $\Sigma_{\mathbf{R}_0}^{at}$ over a fluctuation of the $\rho_{\mathbf{R}_0}^{M_i M_j}$ element, $G_{\mathbf{R}}$ is the inter-site Green's function for the Np-Np bond \mathbf{R} evaluated within the DFT+HI. Once all matrix elements (3) are calculated, they are transformed to the couplings $V_{KK'}^{QQ'}$ between on-site moments (1) as follows:

$$V_{KK'}^{QQ'}(\mathbf{R}) = \sum_{\substack{M_1 M_2 \\ M_3 M_4}} \langle M_1 M_3 | V^{\mathbf{R}} | M_2 M_4 \rangle \quad (4)$$

$$[O_Q^K(J)]_{M_2 M_1} [O_{Q'}^{K'}(J)]_{M_4 M_3},$$

where $[O_Q^K(J)]_{M_1 M_2}$ is the $M_1 M_2$ matrix element of the real spherical tensor defined in accordance with eq. 10 in Santini *et al.*⁸ The SEI matrix \hat{V} shown in Fig. 1b was subsequently obtained by rotating calculated \hat{V} by 45° about the $[010]$ axis thus aligning one of the NN bonds \mathbf{R} with z .

Mean-field calculations and analysis of order parameters. We solved the obtained SE Hamiltonian (2) using the numerical mean-field package MCPHASE⁵⁸ including all $1\mathbf{k}$ structures up to $4 \times 4 \times 4$ unit cells. We have also verified the numerical solution by an analytical approach, Namely, the mean-field equations read

$$\langle \hat{O}_a \rangle = \frac{1}{Z} \text{Tr} \left[\hat{O}_a \exp(-\beta \hat{H}_{MF}^a) \right], \quad (5)$$

where $\hat{H}_{MF}^a = \sum_{b \neq a} \hat{O}_a \hat{V}_{ab} \langle \hat{O}_b \rangle$ is the mean-field Hamiltonian for sublattice a , \hat{V}_{ab} is the SEI matrix between sublattices a and b ($\hat{V}_{ab} = \frac{1}{2} \sum_{[\mathbf{R}_0 + \mathbf{R}] \in b} \hat{V}_{\mathbf{R}}$ with $\mathbf{R}_0 \in a$), $Z = \text{Tr} \left[\exp(-\beta \hat{H}_{MF}^a) \right]$, $\beta = 1/T$. Expanding the RHS of (5) to the linear order in $\langle \hat{O} \rangle$ and allowing for four inequivalent simple-cubic Np sublattices, which is a minimal number needed to cover all possible ordered states on fcc lattice with a NN coupling,⁵⁹ one obtains a system of 60 linear equations. Solutions of the linearized MF equations unambiguously identify primary order parameters. With both numerical and analytical MF approaches

we obtained the highest ordering temperature ($T=38\text{K}$) and lowest free energy for the primary dipole-octupole order displayed in Supplementary Fig. 1.

This order in the $J_{eff} = 3/2$ space was subsequently mapped into the physical $J = 9/2$ space. The J_{eff} density matrix on the inequivalent site a reads $\rho_a(J_{eff}) = \hat{O} \cdot \langle \hat{O} \rangle_a$, where $\langle \hat{O} \rangle_a$ are the corresponding (pseudo) moments. This density matrix is upfolded into the one in the $J = 9/2$ space, neglecting small contributions of the excited $J = 11/2$ and $13/2$ multiplets and renormalizing the Γ_8 CF states accordingly, as $\rho_a(J) = |\Gamma_8\rangle \rho_a(J_{eff}) \langle \Gamma_8|$, where $|\Gamma_8\rangle$ is the CF GS Γ_8 basis, with WFs written as columns in the order of $M = -J_{eff} \dots J_{eff}$. The physical $J = 9/2$ moments are then calculated in the standard way, $\langle O(J)_K^Q \rangle_a = \text{Tr} [\rho_a(J) O(J)_K^Q]$.

Calculations of dynamical susceptibility. In order to calculate the dynamical magnetic susceptibility $\chi_{\alpha\beta}(\mathbf{q}, E)$ we implemented a general RPA approach (see, e. g., Ref. 60). Namely, the general susceptibility matrix in the J_{eff} space reads

$$\bar{\chi}(\mathbf{q}, E) = [I - \bar{\chi}_0(E) \bar{V}_{\mathbf{q}}]^{-1} \bar{\chi}_0(E), \quad (6)$$

where $\bar{\chi}_0(E)$ is the local bare susceptibility, $\bar{V}_{\mathbf{q}}$ is the Fourier transform of SEI matrices $\hat{V}_{\mathbf{R}}$, the bar \dots design-

nate a matrix in combined $[a, \mu]$ indices, where a label inequivalent sublattices, $\mu = [K, Q]$ labels multipoles.

The local susceptibility $\hat{\chi}_{0a}(E)$ for the inequivalent site a is calculated from the MF eigenvalues E^a and eigenstates Ψ^a :

$$\chi_{0a}^{\mu\mu'}(E) = \sum_{AB} \frac{\langle \Psi_A^a | O_\mu | \Psi_B^a \rangle \langle \Psi_B^a | O_{\mu'} | \Psi_A^a \rangle}{E_B^a - E_A^a - E} [p_A^a - p_B^a], \quad (7)$$

where $A(B)$ labels four eigenvalues and eigenstates of the MF Hamiltonian \hat{H}_{MF}^a on the site a , $p_{A(B)}^a$ is the corresponding Boltzmann weight.

Once the J_{eff} susceptibility matrix $\bar{\chi}(\mathbf{q}, E)$ is calculated, it is “unfolded” to the physical $J = 9/2$ space similarly to the $\rho_a(J_{eff})$ density matrix as described above. The magnetic susceptibility $\chi_{\alpha\beta}(\mathbf{q}, E)$ is given by the dipole-dipole blocks of the “unfolded” $\bar{\chi}(\mathbf{q}, E)$ summed over the sublattice indices.

DATA AVAILABILITY

The data that support the findings of this study are available from the corresponding author on reasonable request.

References

- ¹ Haule, K. & Kotliar, G. Arrested Kondo effect and hidden order in URu_2Si_2 . *Nature Physics* **5**, 796 (2009).
- ² Mydosh, J. A. & Oppeneer, P. M. Colloquium: Hidden order, superconductivity, and magnetism: The unsolved case of URu_2Si_2 . *Rev. Mod. Phys.* **83**, 1301–1322 (2011).
- ³ Chandra, P., Coleman, P. & Flint, R. Hysteric order in the heavy-fermion compound URu_2Si_2 . *Nature* **493**, 621 (2013).
- ⁴ Baker, G. A. Singularity structure of the perturbation series for the ground-state energy of a many-fermion system. *Rev. Mod. Phys.* **43**, 479–531 (1971).
- ⁵ Chen, H. H. & Levy, P. M. Quadrupole phase transitions in magnetic solids. *Phys. Rev. Lett.* **27**, 1383–1385 (1971).
- ⁶ Andreev, A. F. & Grishchuk, I. A. Spin nematics. *JETP* **60**, 267 (1984).
- ⁷ Chandra, P. & Coleman, P. Quantum spin nematics: Moment-free magnetism. *Phys. Rev. Lett.* **66**, 100–103 (1991).
- ⁸ Santini, P. *et al.* Multipolar interactions in f -electron systems: The paradigm of actinide dioxides. *Rev. Mod. Phys.* **81**, 807–863 (2009).
- ⁹ Cameron, A. S., Friemel, G. & Inosov, D. S. Multipolar phases and magnetically hidden order: review of the heavy-fermion compound $\text{Ce}_{1-x}\text{La}_x\text{B}_6$. *Reports on Progress in Physics* **79**, 066502 (2016).
- ¹⁰ Sato, T. J. *et al.* Ferroquadrupolar ordering in $\text{PrTi}_2\text{Al}_{20}$. *Phys. Rev. B* **86**, 184419 (2012).
- ¹¹ Tsujimoto, M., Matsumoto, Y., Tomita, T., Sakai, A. & Nakatsuji, S. Heavy-fermion superconductivity in the quadrupole ordered state of $\text{PrV}_2\text{Al}_{20}$. *Phys. Rev. Lett.* **113**, 267001 (2014).
- ¹² Lu, L. *et al.* Magnetism and local symmetry breaking in a mott insulator with strong spin orbit interactions. *Nature Communications* **8**, 14407 (2017).
- ¹³ Hirai, D. & Hiroi, Z. Successive symmetry breaking in a $j_{eff} = 3/2$ quartet in the spin-orbit coupled insulator $\text{Ba}_2\text{MgReO}_6$. *Journal of the Physical Society of Japan* **88**, 064712 (2019).
- ¹⁴ Maharaj, D. D. *et al.* Octupolar versus néel order in cubic $5d^2$ double perovskites. *Phys. Rev. Lett.* **124**, 087206 (2020).
- ¹⁵ Suzuki, M.-T., Magnani, N. & Oppeneer, P. M. Microscopic theory of the insulating electronic ground states of the actinide dioxides AnO_2 ($\text{An} = \text{U, Np, Pu, Am, and Cm}$). *Phys. Rev. B* **88**, 195146 (2013).
- ¹⁶ Osborne, D. W. & Westrum, E. F. The heat capacity of thorium dioxide from 10 to 305 K. the heat capacity anomalies in uranium dioxide and neptunium dioxide. *The Journal of Chemical Physics* **21**, 1884–1887 (1953).
- ¹⁷ Dunlap, B., Kalvius, G., Lam, D. & Brodsky, M. Hyperfine field of ^{237}Np in NpO_2 . *Journal of Physics and Chemistry of Solids* **29**, 1365 – 1367 (1968).
- ¹⁸ Cox, D. & Frazer, B. A neutron diffraction study of NpO_2 . *Journal of Physics and Chemistry of Solids* **28**, 1649 – 1650 (1967).
- ¹⁹ Amoretti, G. *et al.* Neutron-scattering investigation of the electronic ground state of neptunium dioxide. *Journal of Physics: Condensed Matter* **4**, 3459–3478 (1992).

- ²⁰ Mannix, D. *et al.* Unusual magnetism of NpO_2 : A study with resonant x-ray scattering. *Phys. Rev. B* **60**, 15187–15193 (1999).
- ²¹ Tokunaga, Y. *et al.* NMR evidence for triple- \vec{q} multipole structure in NpO_2 . *Phys. Rev. Lett.* **94**, 137209 (2005).
- ²² Erdős, P., Solt, G., Zólierek, Z., Blaise, A. & Fournier, J. M. Magnetic susceptibility and the phase transition of NpO_2 . *Physica B+C* **102**, 164 – 170 (1980).
- ²³ Kopmann, W. *et al.* Magnetic order in NpO_2 and UO_2 studied by muon spin rotation. *Journal of Alloys and Compounds* **271–273**, 463 – 466 (1998).
- ²⁴ Santini, P., Carretta, S., Magnani, N., Amoretti, G. & Caciuffo, R. Hidden order and low-energy excitations in NpO_2 . *Phys. Rev. Lett.* **97**, 207203 (2006).
- ²⁵ Magnani, N. *et al.* Inelastic neutron scattering study of the multipolar order parameter in NpO_2 . *Phys. Rev. B* **78**, 104425 (2008).
- ²⁶ Tokunaga, Y. *et al.* Nmr evidence for higher-order multipole order parameters in NpO_2 . *Phys. Rev. Lett.* **97**, 257601 (2006).
- ²⁷ Sakai, O., Shiina, R. & Shiba, H. Invariant form of hyperfine interaction with multipolar moments - observation of octupolar moments in NpO_2 and $\text{Ce}_{1-x}\text{La}_x\text{B}_6$ by NMR. *Journal of the Physical Society of Japan* **74**, 457–467 (2005).
- ²⁸ Kubo, K. & Hotta, T. Multipole ordering in f -electron systems on the basis of a $j-j$ coupling scheme. *Phys. Rev. B* **72**, 144401 (2005).
- ²⁹ Walstedt, R. E., Tokunaga, Y., Kambe, S. & Sakai, H. NMR evidence for f -electron excitations in the multipolar ground state of NpO_2 . *Phys. Rev. B* **98**, 144403 (2018).
- ³⁰ Paixão, J. A. *et al.* Triple- \vec{q} octupolar ordering in NpO_2 . *Phys. Rev. Lett.* **89**, 187202 (2002).
- ³¹ Magnani, N., Santini, P., Amoretti, G. & Caciuffo, R. Perturbative approach to j mixing in f -electron systems: Application to actinide dioxides. *Phys. Rev. B* **71**, 054405 (2005).
- ³² Fournier, J. M. *et al.* High-energy-neutron spectroscopy of crystal-field excitations in NpO_2 . *Phys. Rev. B* **43**, 1142–1145 (1991).
- ³³ Suzuki, M.-T., Magnani, N. & Oppeneer, P. M. First-principles theory of multipolar order in neptunium dioxide. *Phys. Rev. B* **82**, 241103 (2010).
- ³⁴ Georges, A., Kotliar, G., Krauth, W. & Rozenberg, M. J. Dynamical mean-field theory of strongly correlated fermion systems and the limit of infinite dimensions. *Rev. Mod. Phys.* **68**, 13–125 (1996).
- ³⁵ Anisimov, V. I., Poteryaev, A. I., Korotin, M. A., Anokhin, A. O. & Kotliar, G. First-principles calculations of the electronic structure and spectra of strongly correlated systems: dynamical mean-field theory. *Journal of Physics: Condensed Matter* **9**, 7359 (1997).
- ³⁶ Aichhorn, M. *et al.* TRIQS/DFTTools: A TRIQS application for ab initio calculations of correlated materials. *Computer Physics Communications* **204**, 200–208 (2016).
- ³⁷ Hubbard, J. Electron correlations in narrow energy bands. *Proc. Roy. Soc. (London)* **A 276**, 238 (1963).
- ³⁸ Purovskii, L. V. Two-site fluctuations and multipolar intersite exchange interactions in strongly correlated systems. *Phys. Rev. B* **94**, 115117 (2016).
- ³⁹ Caciuffo, R. *et al.* Multipolar ordering in NpO_2 below 25 K. *Journal of Physics Condensed Matter* **15**, S2287–S2296 (2003).
- ⁴⁰ Caciuffo, R. *et al.* Evidence of a lattice distortion in NpO_2 below 25 K from neutron magnetic inelastic scattering. *Solid State Communications* **79**, 197 – 200 (1991).
- ⁴¹ Lea, K., Leask, M. & Wolf, W. The raising of angular momentum degeneracy of f -electron terms by cubic crystal fields. *Journal of Physics and Chemistry of Solids* **23**, 1381 – 1405 (1962).
- ⁴² Kolorenč, J. c. v., Shick, A. B. & Lichtenstein, A. I. Electronic structure and core-level spectra of light actinide dioxides in the dynamical mean-field theory. *Phys. Rev. B* **92**, 085125 (2015).
- ⁴³ Pi, S.-T., Nanguneri, R. & Savrasov, S. Calculation of multipolar exchange interactions in spin-orbital coupled systems. *Phys. Rev. Lett.* **112**, 077203 (2014).
- ⁴⁴ Wang, B.-T., Shi, H., Li, W. & Zhang, P. First-principles LDA+ U and GGA+ U study of neptunium dioxide. *Phys. Rev. B* **81**, 045119 (2010).
- ⁴⁵ Caciuffo, R. *et al.* Multipolar ordering in NpO_2 below 25 K. *Journal of Physics: Condensed Matter* **15**, S2287–S2296 (2003).
- ⁴⁶ Witczak-Krempa, W., Chen, G., Kim, Y. B. & Balents, L. Correlated quantum phenomena in the strong spin-orbit regime. *Annual Review of Condensed Matter Physics* **5**, 57–82 (2014).
- ⁴⁷ Blaha, P. *et al.* WIEN2k, An augmented Plane Wave + Local Orbitals Program for Calculating Crystal Properties (Karlheinz Schwarz, Techn. Universität Wien, Austria, ISBN 3-9501031-1-2, 2018).
- ⁴⁸ Parcollet, O. *et al.* Triqs: A toolbox for research on interacting quantum systems. *Computer Physics Communications* **196**, 398 – 415 (2015).
- ⁴⁹ Amadon, B. *et al.* Plane-wave based electronic structure calculations for correlated materials using dynamical mean-field theory and projected local orbitals. *Phys. Rev. B* **77**, 205112 (2008).
- ⁵⁰ Aichhorn, M. *et al.* Dynamical mean-field theory within an augmented plane-wave framework: Assessing electronic correlations in the iron pnictide LaFeAsO . *Phys. Rev. B* **80**, 085101 (2009).
- ⁵¹ Purovskii, L. V., Boust, J., Ballou, R., Eslava, G. G. & Givord, D. Higher-order crystal field and rare-earth magnetism in rare-earth- Co_5 intermetallics. *Phys. Rev. B* **101**, 214433 (2020).
- ⁵² Purovskii, L. V. & Khmelevskiy, S. Quadrupolar superexchange interactions, multipolar order, and magnetic phase transition in UO_2 . *Phys. Rev. B* **99**, 094439 (2019).
- ⁵³ Czyżyk, M. T. & Sawatzky, G. A. Local-density functional and on-site correlations: The electronic structure of La_2CuO_4 and LaCuO_3 . *Phys. Rev. B* **49**, 14211–14228 (1994).
- ⁵⁴ Purovskii, L. V., Amadon, B., Biermann, S. & Georges, A. Self-consistency over the charge density in dynamical mean-field theory: A linear muffin-tin implementation and some physical implications. *Phys. Rev. B* **76**, 235101 (2007).
- ⁵⁵ Aichhorn, M., Purovskii, L. & Georges, A. Importance of electronic correlations for structural and magnetic properties of the iron pnictide superconductor LaFeAsO . *Phys. Rev. B* **84**, 054529 (2011).
- ⁵⁶ Delange, P., Biermann, S., Miyake, T. & Purovskii, L. Crystal-field splittings in rare-earth-based hard magnets: An ab initio approach. *Phys. Rev. B* **96**, 155132 (2017).
- ⁵⁷ Sunko, V. *et al.* Probing spin correlations using angle-resolved photoemission in a coupled metallic/mott insula-

tor system. *Science Advances* **6** (2020).

- ⁵⁸ Rotter, M. Using mcphase to calculate magnetic phase diagrams of rare earth compounds. *Journal of Magnetism and Magnetic Materials* **272-276, Supplement**, E481 – E482 (2004).
- ⁵⁹ Smart, J. P. *Effective Field Theories of Magnetism* (W. B. Saunders Company, Philadelphia, 1966).
- ⁶⁰ Rotter, M., Le, M. D., Boothroyd, A. T. & Blanco, J. A. Dynamical matrix diagonalization for the calculation of dispersive excitations. *Journal of Physics: Condensed Matter* **24**, 213201 (2012).

ACKNOWLEDGMENTS

L.V.P. acknowledges support by the European Research Council grants ERC-319286-”QMAC” and the

computer team at CPHT. S.K. is grateful to Ecole Polytechnique for financial support and to CPHT for its hospitality.

AUTHOR CONTRIBUTIONS

L.V.P. carried out the *ab initio* calculations and INS spectra simulations. S. K. carried out the order parameters’ analysis. Both authors contributed equally to solving the mean-field equations, analysis of the results and writing of the manuscript.

COMPETING INTERESTS

The authors declare no competing interests.